CONFIDENTIAL

RM L53I25a

Copy
RM L53I25a

NACA RM L53I25a

NACA

RESEARCH MEMORANDUM

FLIGHT DETERMINATION OF DRAG OF NORMAL-SHOCK NOSE INLETS WITH VARIOUS COWLING PROFILES AT MACH NUMBERS FROM 0.9 TO 1.5

By R. I. Sears, C. F. Merlet, and L. W. Putland

Langley Aeronautical Laboratory
Langley Field, Va.

CLASSIFIED DOCUMENT

NATIONAL ADVISORY COMMITTEE
FOR AERONAUTICS

WASHINGTON

October 22, 1953

CONFIDENTIAL

NATIONAL ADVISORY COMMITTEE FOR AERONAUTICS

RESEARCH MEMORANDUM

FLIGHT DETERMINATION OF DRAG OF NORMAL-SHOCK NOSE INLETS WITH VARIOUS COWLING PROFILES AT MACH NUMBERS FROM 0.9 TO 1.5

By R. I. Sears, C. F. Merlet, and L. W. Putland

SUMMARY

Free-flight tests were made with normal-shock nose-inlet models with 1-series, parabolic, and conic cowling profiles to investigate the external drag characteristics at an angle of attack of 0°. The Mach number range of the tests was from 0.9 to 1.5; the mass-flow ratio, from 0.7 to 1.0; and the Reynolds number based on body maximum diameter varied from 2.5×10^6 to 5.5×10^6. Two related nonducted bodies were also tested for comparison purposes.

At maximum flow rate the inlet models had about the same external drag at a Mach number of approximately 1.1 but at higher Mach numbers the conic cowl had the least drag. Blunting or beveling the lip of the conic cowl while keeping the fineness ratio constant resulted in a slightly higher drag than for the sharp-lip conic cowl at maximum flow rate, but at a mass-flow rate of 0.8 the blunt-, beveled-, and sharp-lip conic cowls and the parabolic cowl all had about the same drag. The higher drag of the NACA 1-49-300 cowling compared with the blunt-lip conic cowl is associated with the greater fullness back of the inlet.

INTRODUCTION

Because the total-pressure recoveries attainable with normal-shock inlets at Mach numbers up to about 1.4 are as good as, or better than, those for other types of inlets, normal-shock inlets are of real interest for aircraft at low supersonic speeds. References 1 to 3 present data which indicate large differences in drag at Mach numbers of approximately 1.4 for normal-shock inlets of different geometry, whereas data summarized in reference 4 show large effect on drag due to inlet proportions at Mach number of approximately 1.1.

The Pilotless Aircraft Research Division of the Langley Laboratory has therefore undertaken a program to investigate the drag characteristics of normal-shock inlets of various nose geometry. The first phase of this program is concerned with the effects of nose profile and the results are reported herein. A flight technique, differing from that previously used for ducted models, was developed in order to obtain a little information from each of many models rather than more extensive information about only a few models.

Two related nonducted bodies were tested for purposes of comparison with the normal-shock nose-inlet data. Although the models of the present investigation are all nose-inlet models, it is expected that many of the results might also be applicable in the design of scoop inlets.

SYMBOLS

A	area, sq ft
A_{cr}	critical area: area at which sonic velocity will be obtained, assuming one-dimensional isentropic process, sq ft
C_D	drag coefficient, $\frac{D}{\frac{1}{2}\rho_o V_o^2 A_f}$
C_p	pressure coefficient, $\frac{p - p_o}{\frac{1}{2}\rho_o V_o^2}$
D	drag, lb
g	acceleration of gravity, 32.2 ft/sec^2
H	total pressure
H_s	pitot-stagnation pressure
M	Mach number
m/m_o	ratio of mass flow of air through the duct to mass flow of air through a free-stream tube of area equal to inlet area
p	static pressure
R	Reynolds number, based on 7.00-inch body diameter

r	radius, in.
V	velocity
W	weight of the model
X	longitudinal distance, measured from the maximum-diameter station, positive downstream, in.
γ	ratio of specific heats, 1.40 for air
ρ	air density
θ	flight-path angle

Subscripts:

0	free stream
1	first minimum-area station
f	frontal
i	inlet, at lip leading edge
e	exit
int.	internal
x	external
T	total

MODELS

Ducted-nose-inlet models having six different cowl shapes were tested as part of the investigation reported herein. Three models of each cowl shape were tested, each model having a different flow rate. The only difference in the external geometry of the three models for each cowl shape was a slight difference in length, the afterbody being cut off at the station required to give the desired exit area.

Five of the cowls were of fineness ratio 3 and had an inlet area 24 percent of the body frontal area. The sixth cowl was of fineness ratio 2.5 and had an inlet area 16 percent of the body frontal area. Two related, nonducted bodies of revolution were tested, one for each

cowl fineness ratio investigated. The external profiles shall be designated by Roman numerals, whereas the internal configurations shall be referred to by Arabic numbers.

The general arrangement of the three model configurations tested for a typical fineness-ratio-3 cowl and the related nonducted body is shown in figure 1. Similar information is presented in figure 2 for the fineness-ratio-2.5 cowl models. All models had identical fins and afterbody lines.

The afterbody is defined by a parabolic arc with its vertex at the maximum-diameter station. It is similar to that used in the inlet investigation reported in references 1 and 2. The coordinates are listed in table I. All afterbodies were spun on the same die from 0.09-inch magnesium and finished to a smooth, fair contour and formed the afterportion at the duct. The length at which the afterbody was cut off for each flow rate is shown on figures 1 and 2.

Each model was stabilized by four 60° delta fins having a total exposed area 3.2 times the body frontal area. The airfoil section was hexagonal and was fabricated from 1/8-inch magnesium sheet by beveling the leading and trailing edges.

The nonducted models shown in figures 1 and 2 were related to the ducted models in that coordinates of the duct lips were also coordinates of the nonducted bodies. Thus, the nonducted forebody was defined by a parabolic arc with its vertex at the maximum diameter and passing through the inlet lip. Coordinates are listed in table I.

Details of the various cowl shapes tested are shown in figure 3, and coordinates are given in table I. Cowl I had the NACA 1-49-300 profile (ref. 5). Cowl II had a parabolic profile, obtained by cutting off at the inlet station the nose of the nonducted body A shown at the top of figure 1. The external lip angle was 9.8°. Cowls III, IV, and V are called conic because all cowl III and the major part of the contour of cowls IV and V were defined by a truncated cone. The cone half angle was 4.9° for cowl III and 4.4° for cowls IV and V. Cowl III had sharp lips, the external lip angle being 4.9°. Cowl IV had a beveled lip of external angle 9.8°, the contour in the region of the lips being identical with that of the parabolic cowl II. Cowl V had blunt lips with an external lip angle of 90°. The contour in the region of the lips was identical with that of the 1-series cowl I. Cowl VI had the NACA 1-40-250 profile.

The external profiles in the region of the lips of the five fineness-ratio-3 cowls are better compared in figure 4. The three arrangements of internal lines in the region of the inlet designated by the configuration numbers 1, 2, and 3, and used with each cowl shape to regulate the internal air flow are also shown in figure 4. For each cowl shape the internal

contraction ratios used were 1.00, 0.83, and 0.67 for configurations 1, 2, and 3, respectively. A similar arrangement, using contraction ratios of 1.00, 0.75, and 0.56, was used for cowl VI which had a smaller inlet area. The minimum section of all models was a cylindrical section 1/2-inch long, and the internal lips of the models with a contraction ratio less than 1.00 were parabolic from the lip to the minimum section. No attempt was made to measure total-pressure recovery. Details of the diffuser shape are not considered pertinent to this drag investigation and are not presented.

Photographs of the models showing each cowl shape and nonducted body tested are given in figure 5, and the major physical characteristics of the models are presented in tabular form in table II.

TESTS AND TECHNIQUES

Three models were flown for each normal-shock inlet-cowl shape in order to obtain the variation of C_D with m/m_o. Different rocket motors were used during the course of the investigation; this fact largely accounts for the different maximum Mach numbers to which data were obtained for the various models. The range of variation of Reynolds number with Mach number is shown in figure 6 for the models tested. All models were flown on a zero-lift trajectory and the data presented are for an angle of attack of 0°.

In order to facilitate building and flight-testing models of many different inlet geometries, all but three of the models were built without telemeters. Total drag was obtained over the flight Mach number range from computations based on the CW Doppler radar velocity measurements, the flight path indicated by the NACA modified SCR 584 tracking radar and radiosonde observations. Corrections were made for the horizontal component of the wind velocity and for flight-path curvature. A telemeter was used with nonducted model B to determine the base pressure; with model cowl II, configuration 3, to measure the static pressures at the inlet minimum-area station, the exit, and at two stations on the afterbody; and with model cowl VI, configuration 3, to measure three afterbody static pressures.

The model internal geometry was made such that at supersonic speeds the inlet was started or choking occurred at the minimum area just back of the inlet, while the exit was choked for all cases. The exit area of each ducted model was made equal to 1.05 times the inlet minimum area in order that the exit would stay choked to as low a free-stream Mach number as possible to permit evaluation of the internal drag. The duct was made cylindrical for at least 1.2 exit diameters ahead of the exit to aid in providing uniform static pressure at the exit. The fairly large contraction

of at least 4 to 1 from near the maximum-diameter station to the exit assured sonic rather than supersonic exit velocities and also helped in providing uniform total pressure at the exit. The entering mass flow and the internal drag can, therefore, be calculated for the Mach number range over which these choking conditions existed. The details of making these calculations are presented in the appendix.

Figure 7 compares the values of C_{D_i} and m/m_o calculated as indicated in the appendix with values computed from measurements made with telemetered model, cowl II, configuration 3. The good agreement shown is believed to justify use of the calculated results at $M_o \geq 0.9$, although at subsonic speeds some of the assumptions involved are not quite fulfilled.

ACCURACY OF DATA

The accuracy of the data is estimated to be within the following limits:

m/m_o, for $M \geq 1.0$	± 0.01
C_{D_X}	± 0.01
C_p	± 0.015
M	± 0.01

RESULTS AND DISCUSSION

Effect of Afterbody Length

Because the afterbody length was slightly greater for the models admitting lesser mass flow, it is necessary to examine the differences in C_{D_X} associated with differences in model length. Figure 8 presents measured afterbody pressure coefficients for two ducted models as a function of Mach number. The static-pressure orifices were located at the body stations shown on the figure, on a longitudinal line that passed midway between two fins.

The data of reference 6 indicate that large changes in nose shape have negligible effect on the pressures over the rearward 5 percent of the body length. It is, therefore, assumed that the differences in C_p shown in figure 8 are caused primarily by the differences in afterbody length, the effect of the exit and of the jet propagating upstream through the boundary layer at supersonic Mach numbers or through the subsonic flow field at the exit in the lower range of test Mach numbers.

Integration of the measured pressures to obtain a pressure drag coefficient for the portion of each model rearward of station 34 (where

both models had nearly the same pressure coefficient) gave the same value for each model, within $\Delta C_D = 0.001$. The coefficient of skin-friction drag acting on the incremental surface area of the longer afterbody is estimated to be 0.002. It is, therefore, believed that any differences in C_{D_X} caused by varying the length of the afterbody are small and well within the accuracy of measuring C_{D_X}.

Basic Data

The curves of external drag for each ducted model are presented in figure 9. The mass-flow ratio associated with each drag curve is also given. For configuration 1 with each cowl the mass-flow ratio was unity at all Mach numbers; that is, no air was spilled. An increasing amount of air was spilled with configurations 2 and 3. The inlet-contraction ratios of configurations 2 and 3 were too great to permit the inlets to start in the test Mach number range.

The curves of total drag as a function of Mach number are given in figure 10 for the two nonducted models. Base drag was measured for nonducted model B only and is also shown on figure 10.

Effect of Cowl Shape

The drag-coefficient curves at $m/m_o = 1.0$ for the various normal-shock inlet models having fineness-ratio-3 cowls are shown superimposed in figure 11 for comparison purposes. Also shown is the total-minus-base drag-coefficient curve for solid body model A and the curve of fin drag coefficient estimated from the data of reference 7. The base drag coefficient of model A was obtained by using the measured base pressure coefficient of model B.

Inspection of this figure indicates that in the transonic range below $M \approx 1.1$ all the ducted models with fineness-ratio-3 cowlings have about the same drag coefficient. As the Mach number increases the curves diverge, the sharp-lip conic cowl having the least drag and the 1-series cowl the greatest. Comparison of the drag of the three conic cowl models at $M > 1.2$ indicates that, for these cowls of constant fineness ratio, beveling or blunting the lip caused a small increase in drag over that of the sharp-lip conic cowl. It should be noted, however, that of the two conic cowls which were identical except for lip shape, cowls IV and V, the blunt-lip conic cowl had slightly lower drag than the beveled-lip conic cowl. Thus, it appears that the effect of lip bluntness on drag is critically dependent on the manner of blunting the lip. Because the 1-series cowl and the blunt-lip conic cowl had the same external lines in the region of the inlet lip, it is apparent that the higher drag of the 1-series cowl is associated with its greater fullness farther rearward.

The drag of the pointed nonducted body is greater than that of all the inlet models in the transonic range and at $M > 1.2$ is about equal to that of the cowling which was defined by the same parabolic arc. This result is consistent with data presented in reference 2 for another nose inlet. At all test Mach numbers greater than 1.05, the drag of the conic-cowl models was less than that of the solid body for mass-flow ratios greater than 0.9. The data of reference 8 indicate that the solid body is a low-drag configuration at supersonic speeds. The lower drags obtained with the conic cowls indicate therefore that these also must be considered as real low-drag configurations.

The variation of external drag coefficient with mass-flow ratio at $M = 1.3$ is shown for the various cowls in figure 12 by crossplotting the data of figure 9. The increase in drag with spillage is different for each cowl, it being greatest for the conic cowl with sharp lips and least for the 1-series cowl I. At $m/m_o = 0.8$, the three conic cowls and the parabolic cowl all have about the same drag. The 1-series cowl because of its high drag at maximum-flow rate has the greatest drag at all flow rates tested.

The rate of increase of drag coefficient with spillage for the various cowls is better compared in figure 13 where the slopes of the curves of figure 12 and similar ones for other Mach numbers are shown for each cowl. The slope of the additive drag curve computed by assuming one-dimensional flow is also shown as a function of Mach number. The departure of the curves of figure 13 from the additive drag curve is caused by the reductions in cowl pressure drag with spillage. The data indicate very little change in cowl pressure drag with spillage for the sharp-lip inlet and large reductions for the 1-series inlet. This trend is consistent with previous experiences with leading-edge suction for wings at angle of attack. Cowl pressure distributions at several flow rates are shown in reference 6 for 1-series cowls and in reference 3 for a conical cowl with beveled lip.

NACA 1-40-250 Cowl

The models with NACA 1-40-250 cowl and the related nonducted body B were tested for purpose of comparison of results with those reported in reference 1. These models and those of reference 1 differed only in fin geometry and overall length. The flight-test technique for obtaining the data was considerably different from that reported herein. Comparison of the data of figures 9(f) and 10 with that presented in reference 1 indicates that, when allowance is made for the differences in fin drag, the measured drag results of the present tests are essentially the same as those of reference 1 for both the ducted and nonducted models. A comparison of the results for the ducted models is shown in figure 14 for several Mach numbers. The solid curve is the external drag as presented

in reference 1, extrapolated to $m/m_o = 1.0$. The points are the measured values obtained for cowl VI of this investigation. The dashed curve was obtained by correcting the data of reference 1 for the difference in fin-plus-interference drag. The difference in fin-plus-interference drag was obtained by subtracting the total-minus-base drag of nonducted model B from the total-minus-base drag of the solid body of reference 1.

Comparison of the minimum drag of the NACA 1-40-250 nose-inlet model with the minimum drag of the 1-49-300 model (cowl I) shows that the subsonic drags were essentially the same, but for $M > 1.02$, the shorter, blunter, NACA 1-40-250 cowl had the higher drag. This effect of inlet proportion is in agreement with data summarized in reference 4 for a number of NACA 1-series inlets.

CONCLUSIONS

Models having normal-shock nose inlets with 1-series, parabolic, and conic cowls have been tested at Mach numbers from 0.9 to 1.5 and flow ratio from 0.7 to 1.0 at an angle of attack of 0^o. Two related nonducted bodies were also tested for comparison purposes. Within the range of the tests, the following conclusions apply:

1. At the maximum flow rate, the conic, parabolic, and 1-series cowls all had about the same external drag at a Mach number of approximately 1.1. At higher Mach numbers, the drag of the conic cowl was appreciably less than that of the parabolic or 1-series cowls.

2. Blunting or beveling the lip of the conic cowl while keeping the cowl fineness ratio constant resulted in drag coefficients slightly higher than for the sharp-lip conic cowl at maximum flow rate. At a mass-flow ratio of about 0.8, the conic cowls with sharp, blunt, or beveled lips and the parabolic cowl all give about the same drag. The higher drag at the NACA 1-49-300 cowl compared with the blunt-lip conic cowl is associated with its greater fullness back of the inlet.

3. The sharp-lip conic cowl experienced only small reductions in cowl pressure drag with air spillage, whereas the 1-series cowl had large reductions. Because of its high drag at maximum flow rate, however, the 1-series cowl gave the greatest drag at all flow rates of all the cowls tested at Mach number greater than 1.1.

4. The drag of the conic cowl models at high mass-flow rates was less than that of a related parabolic nonducted model at Mach number

greater than 1.05. At Mach number greater than 1.2, the drag of the parabolic-cowl model was about the same as that of the nonducted model.

Langley Aeronautical Laboratory,
National Advisory Committee for Aeronautics,
Langley Field, Va., September 8, 1953.

APPENDIX

NORMAL-SHOCK INLETS

The total drag was obtained from the CW Doppler radar and the SCR 584 tracking radar measurements of velocity and flight path, respectively. Thus,

$$D_T = -W\left(\frac{1}{g}\frac{dV}{dt} + \sin\theta\right) \tag{A1}$$

The external drag, defined in the usual manner as the sum of the dragwise component of the aerodynamic pressure and viscous forces acting on the external surface of the body plus the dragwise component of the aerodynamic pressure forces acting on the external contour of the entering streamline, was obtained by subtracting the internal drag from the total drag. Thus,

$$D_x = D_T - D_{int.} \tag{A2}$$

The internal drag is obtained by applying the momentum equation between the free stream ahead of the model and the duct exit.

$$D_{int.} = \gamma p_o M_o^2 A_o - \gamma p_e M_e^2 A_e - \left(p_e - p_o\right) A_e \tag{A3}$$

where for $M_o < M_{o_{start}}$, if it is assumed that $M_1 = 1$ and $H_1 = H_s$,

$$A_o = \frac{H_s/H_o}{\left(A_{cr}/A\right)_o} A_1 \tag{A4a}$$

and for $M_o \geq M_{o_{start}}$:

$$A_o = A_i \tag{A4b}$$

and since $M_e = 1$,

$$p_e = 0.528H_o \frac{A_o}{A_e}\left(\frac{A_{cr}}{A}\right)_o \tag{A5}$$

The mass-flow ratio is

$$m/m_o = \frac{\rho_o A_o V_o}{\rho_o A_i V_o} = \frac{A_o}{A_i} \tag{A6}$$

Obviously the mass flow and internal drag can be properly evaluated in the manner indicated only for the range of M_o for which the flow follows the assumed pattern. The data of reference 2 show that for a normal-shock nose inlet the mass flow computed in the manner indicated is in excellent agreement with the independently measured values of mass flow when the inlet is choked or started.

The minimum Mach number for which the inlet and exit will be choked depends on the relative size of the minimum area at the inlet and exit and on the internal losses. The models of the present investigations were designed to choke at both the inlet and exit at Mach numbers from slightly above sonic to the maximum attained.

One ducted model with pressure instrumentation and telemeter was flight-tested to determine the minimum Mach number at which the assumed choking conditions existed at the inlet and exit. The measured inlet and exit static pressures together with the pitot stagnation pressure at the inlet were used to evaluate the internal drag and mass flow for this model. The method of reducing these data was the same as that discussed in reference 1 for ducted-nose-inlet models with telemeters.

The pressure measurements indicated that the inlet and exit were choked for values of M_o greater than 1.03 and 1.08, respectively. The data of figure 7, however, show that the mass flow and internal drag computed according to equations 1 to 6 is in excellent agreement with the measured values at all supersonic Mach numbers. At $M = 0.9$ the computed C_{D_i} is still in good agreement with the measured value and the computed m/m_o is about 0.015 greater than that measured. It is, therefore, believed that the method of calculation gives the correct values of C_{D_i} and m/m_o at $M > 1.03$. For Mach numbers from 0.9 to 1.03, a small error is introduced in the magnitude of m/m_o only.

REFERENCES

1. Sears, Richard I., and Merlet, C. F.: Flight Determination of the Drag and Pressure Recovery of an NACA 1-40-250 Nose Inlet at Mach Numbers From 0.9 to 1.8. NACA RM L50L18, 1951.

2. Sears, Richard I., and Merlet, C. F.: Flight Determination of Drag and Pressure Recovery of a Nose Inlet of Parabolic Profile at Mach Numbers From 0.8 to 1.7. NACA RM L51E02, 1951.

3. Fraenkel, L. E.: The External Drag of Some Pitot-Type Intakes at Supersonic Speeds: Part II. Rep. No. Aero. 2422, British R.A.E., June 1951.

4. Pendley, Robert E., Milillo, Joseph R., Fleming, Frank F., and Bryan, Carroll R.: An Experimental Study of Five Annular-Air-Inlet Configurations at Subsonic and Transonic Speeds. NACA RM L53F18a, 1953.

5. Baals, Donald D., Smith, Norman F., and Wright, John B.: The Development and Application of High-Critical-Speed Nose Inlets. NACA Rep. 920, 1948. (Supersedes NACA ACR L5F30a.)

6. Pendley, Robert E., Milillo, Joseph R., and Fleming, Frank F.: An Investigation of Three NACA 1-Series Nose Inlets at Subsonic and Transonic Speeds. NACA RM L52J23, 1953.

7. Hopko, Russell N., and Sandahl, Carl A.: Free-Flight Investigation of the Zero-Lift Drag of Several Wings at Supersonic Mach Numbers Extending to 2.6. NACA RM L52D29, 1952.

8. Hart, Roger G., and Katz, Ellis R.: Flight Investigation at High-Subsonic, Transonic, and Supersonic Speeds To Determine the Zero-Lift Drag of Fin-Stabilized Bodies of Revolution Having Fineness Ratios of 12.5, 8.91, and 6.04 and Varying Positions of Maximum Diameter. NACA RM L9I30, 1949.

TABLE I.- EXTERNAL COORDINATES

Nonducted model (from maximum diameter)

Model A forebody	
x	r
-29.40	0
-28.90	.12
-28.40	.23
-28.00	.33
-27.00	.55
-25.00	.97
-20.00	1.88
-15.00	2.59
-10.00	3.10
-5.00	3.40
0	3.50

Model B forebody	
x	r
-25.20	0
-24.20	.27
-23.20	.53
-22.20	.78
-21.20	1.02
-20.20	1.25
-18.20	1.67
-15.20	2.23
-10.20	2.93
-5.20	3.35
0	3.50

Afterbody	
x	r
0	3.50
5.60	3.45
10.27	3.34
15.87	3.14
21.47	2.84
24.27	2.65
30.80	2.15
35.70	1.68
42.70	.90

Normal-shock inlet models - forebody (from maximum diameter)

Cowl I	
x	r
-21.00	1.71
-20.79	1.90
-20.37	2.04
-19.95	2.15
-17.85	2.52
-14.70	2.87
-10.50	3.19
-6.30	3.39
0	3.50

Cowl II	
x	r
-21.00	1.71
-20.00	1.88
-19.00	2.04
-18.00	2.19
-17.00	2.33
-15.00	2.59
-10.00	3.10
-5.00	3.40
0	3.50

Cowl III	
x	r
-21.00	1.71
-10.00	2.65
0	3.50

Cowl IV	
x	r
-21.00	1.71
-20.00	1.88
-19.00	2.04
0	3.50

Cowl V	
x	r
-21.00	1.71
-20.92	1.83
-20.79	1.90
0	3.50

Cowl VI	
x	r
-17.50	1.40
-17.40	1.57
-17.24	1.67
-17.06	1.75
-16.63	1.91
-14.88	2.35
-10.50	2.97
-5.25	3.37
0	3.50

TABLE II.- PHYSICAL CHARACTERISTICS OF THE MODELS

Symbol	Designation	Forebody profile	Forebody fineness ratio	External lip angle (deg)	Inlet contraction ratios tested for configurations -		
					1	2	3
I	1-49-300	NACA 1-series	3.0	90	1.0	0.83	0.67
II	Parabolic	Parabolic	3.0	9.8	1.0	.83	.67
III	Conic, sharp lip	Conic, 4.9° half-angle	3.0	4.9	1.0	.83	.67
IV	Conic, beveled lip	Conic, 4.4° half-angle	3.0	9.8	1.0	.83	.67
V	Conic, blunt lip	Conic, 4.4° half-angle	3.0	90	1.0	.83	.67
VI	1-40-250	NACA 1-series	2.5	90	1.0	.75	.56
A	Nonducted model A	Parabolic	4.2	----	---	----	----
B	Nonducted model B	Parabolic	3.6	----	---	----	----

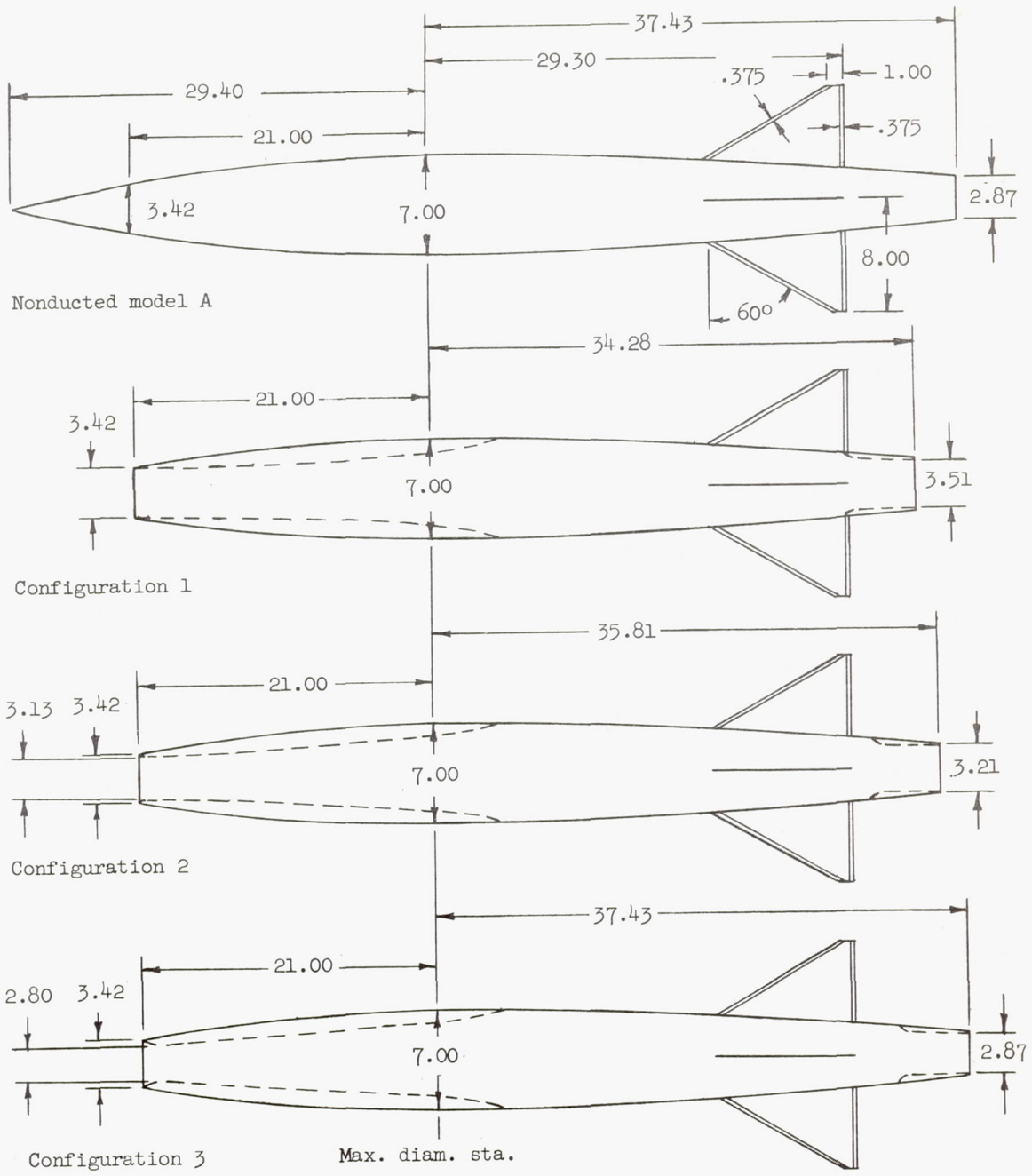

Figure 1.- General arrangement of ducted models with fineness-ratio-3 cowls and related nonducted model. All dimensions are in inches.

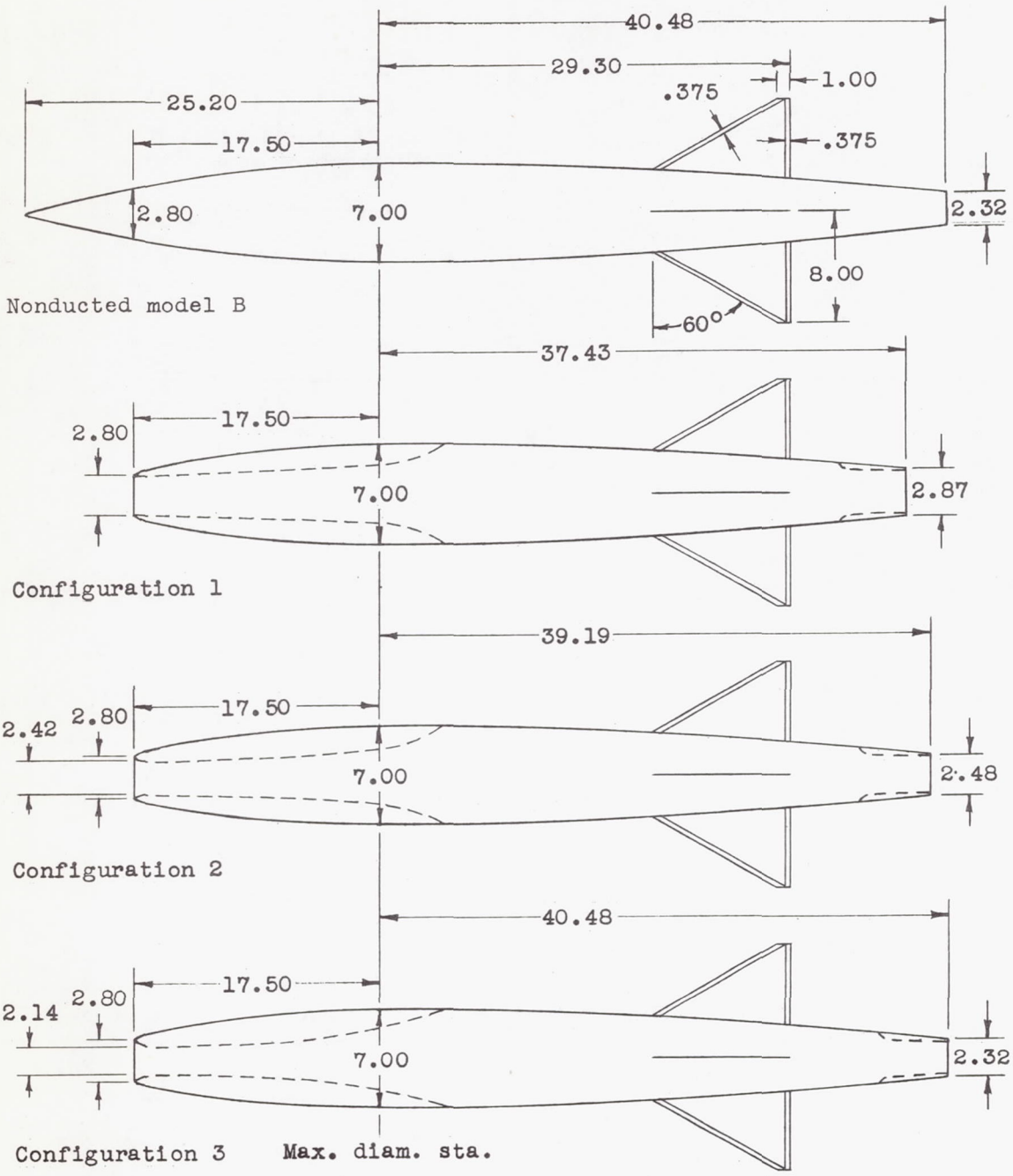

Figure 2.- General arrangement of ducted models with fineness-ratio-2.5 cowls and related nonducted model. All dimensions are in inches.

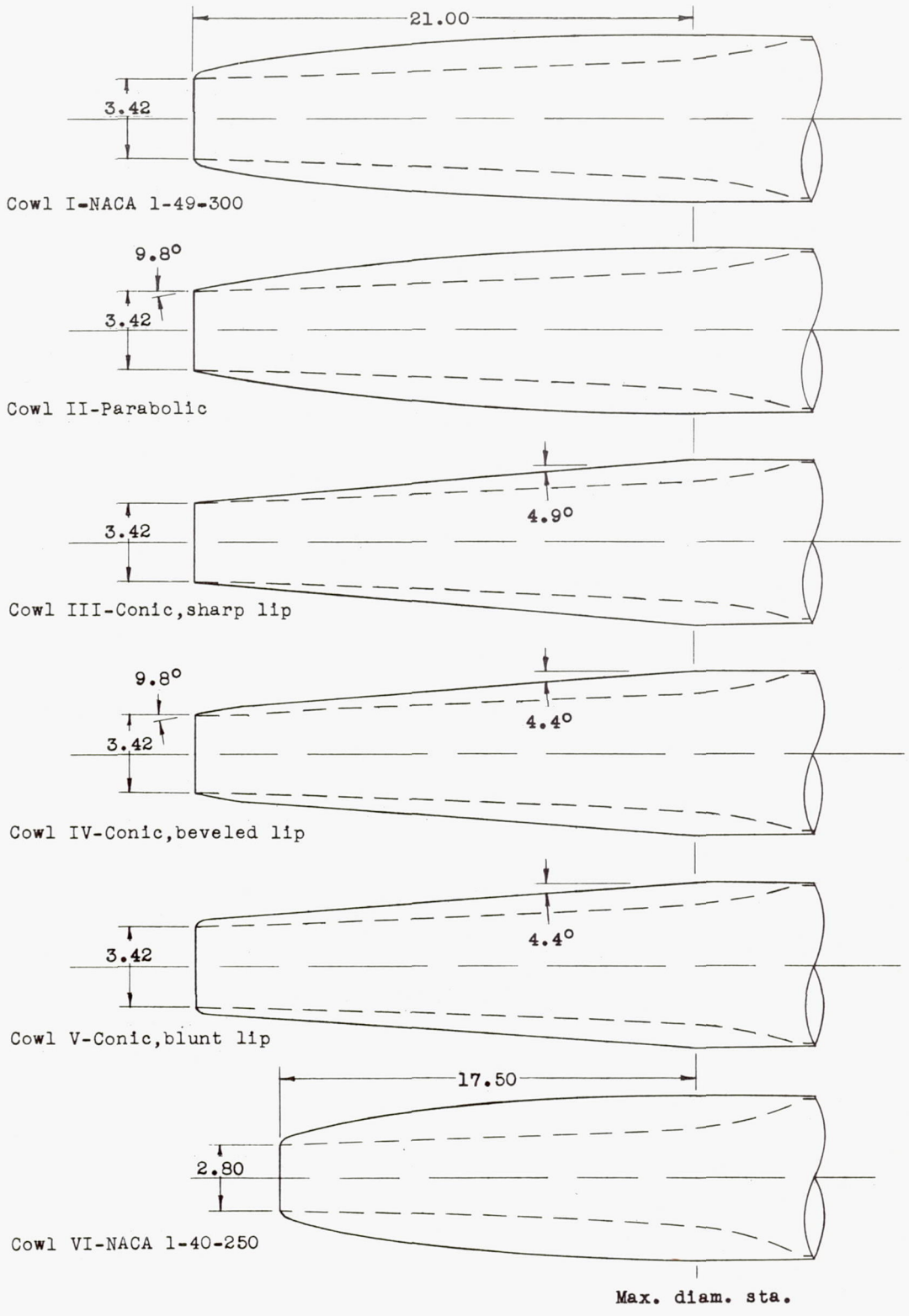

Figure 3.- Details of cowl shapes. All dimensions are in inches.

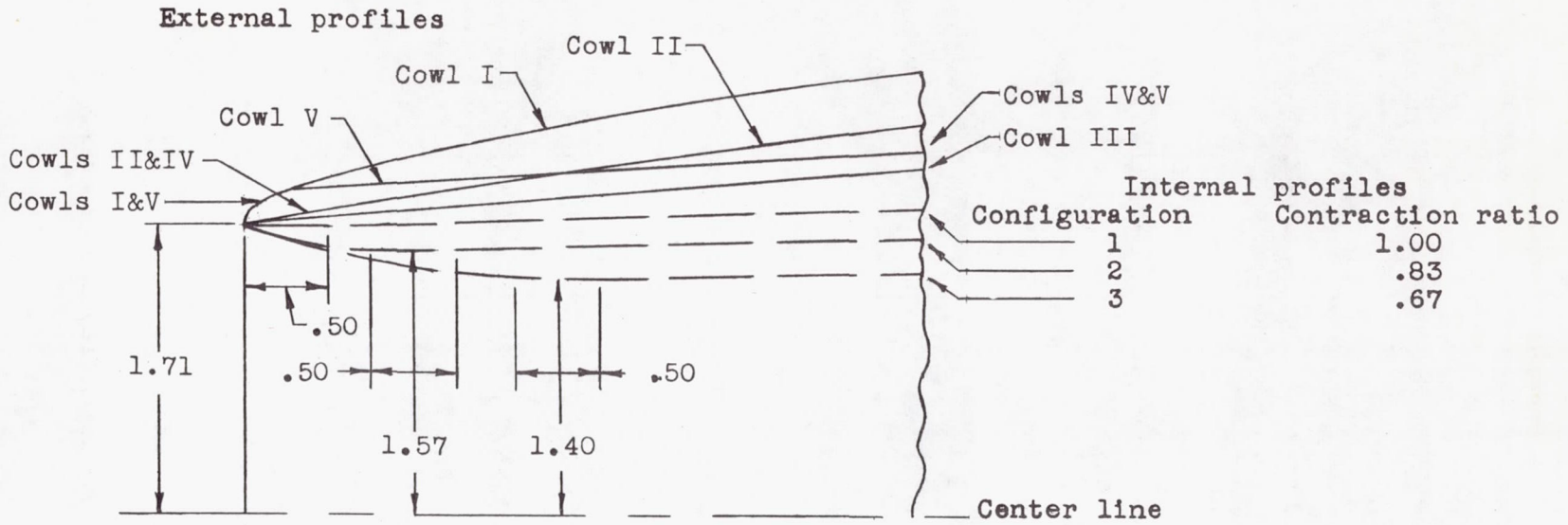

Figure 4.- Details of lip shapes of fineness-ratio-3 cowls. All dimensions are in inches.

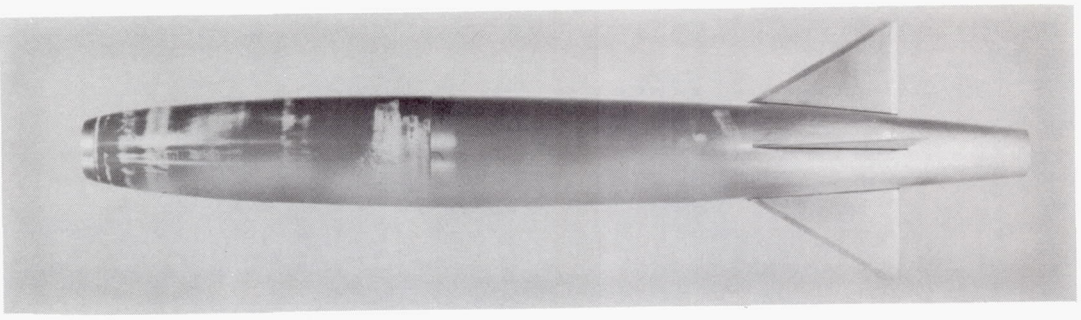

Cowl I-NACA 1-49-300 L-72410.1

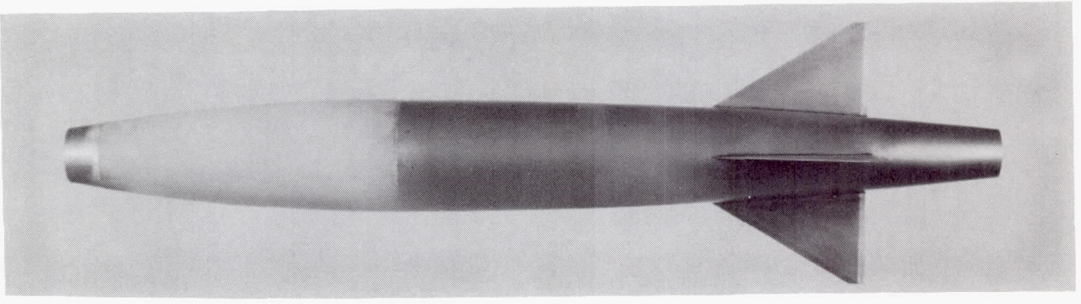

Cowl II-Parabolic L-71587.1

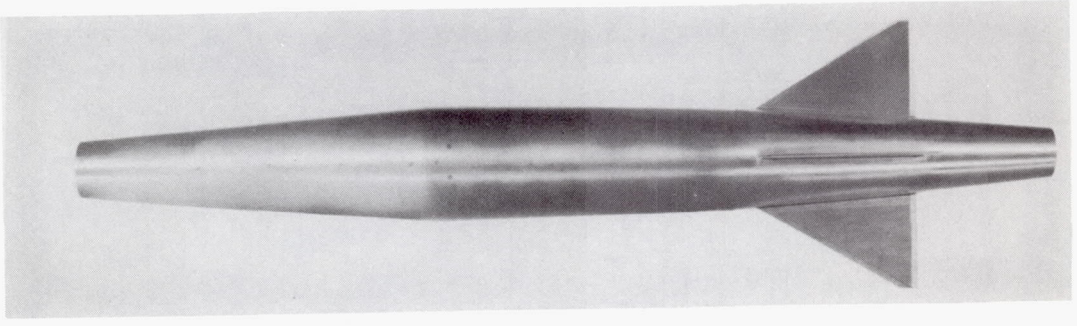

Cowl III-Conic, sharp lip L-73586.1

(a) General views of ducted models.

Figure 5.- Photographs of models.

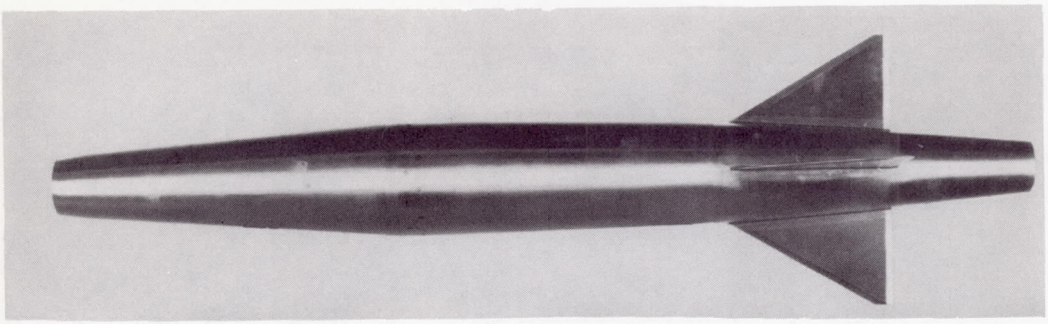

Cowl IV-Conic, beveled lip L-73636.1

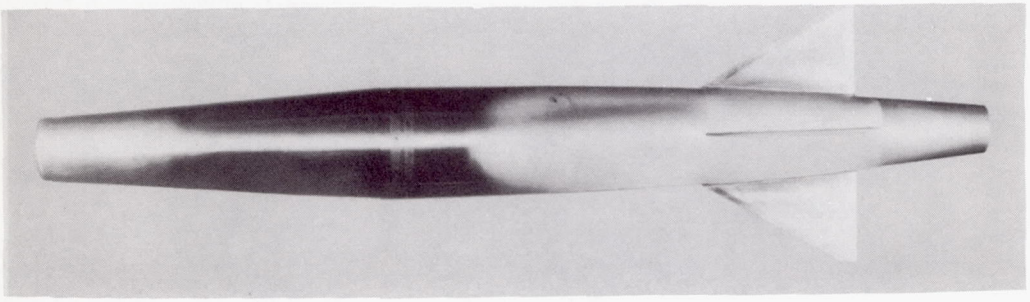

Cowl V-Conic, blunt lip L-75517.1

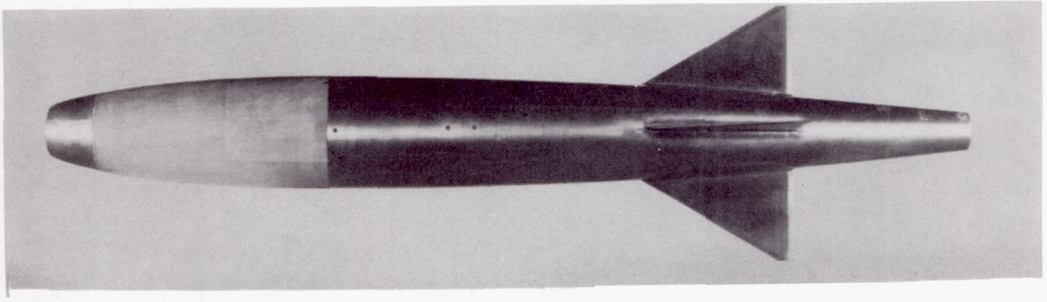

Cowl VI-NACA 1-40-250 L-75361.1

(a) Concluded.

Figure 5.- Continued.

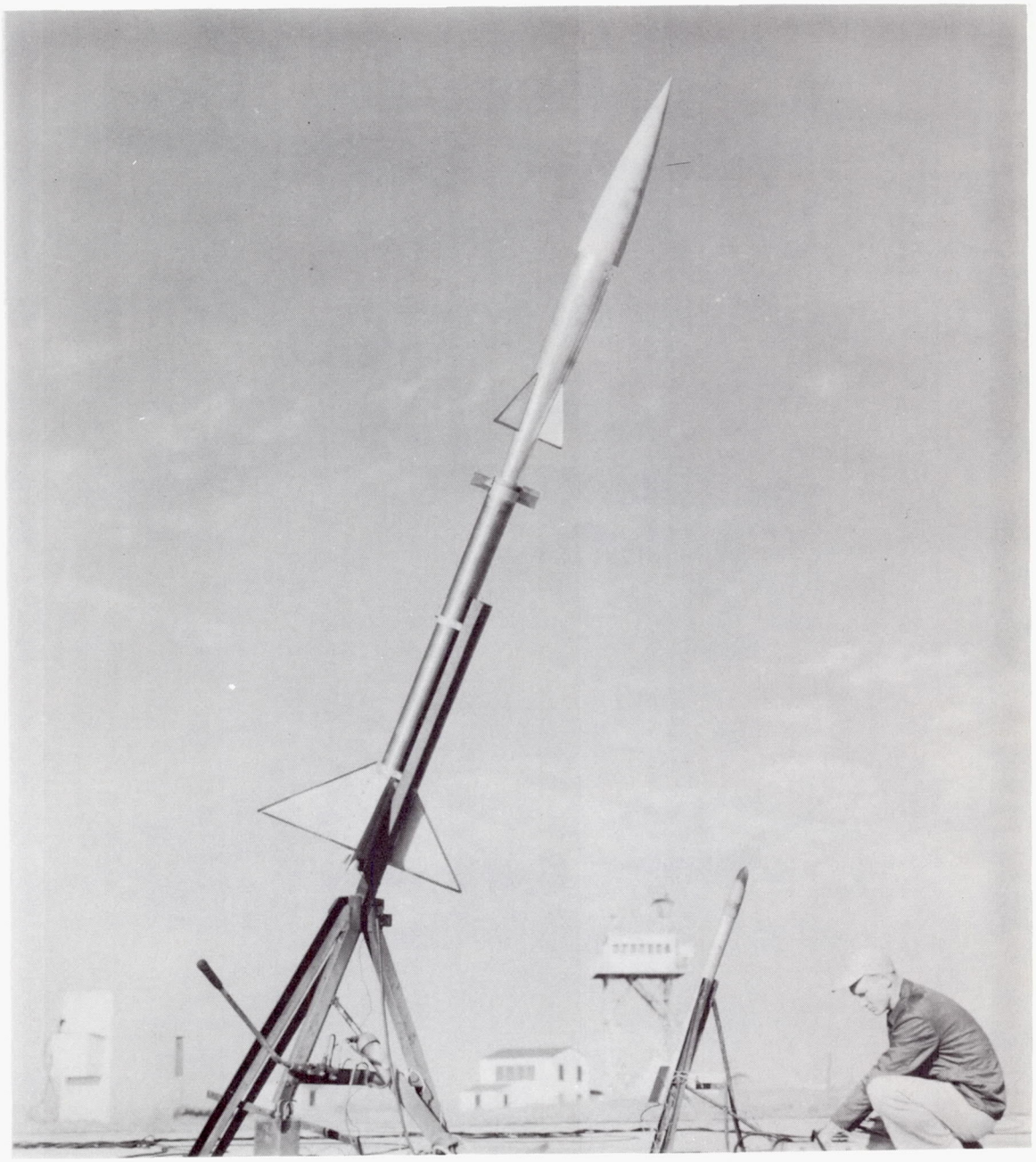

L-73803.1

(b) Nonducted model A on the launcher.

Figure 5.- Concluded.

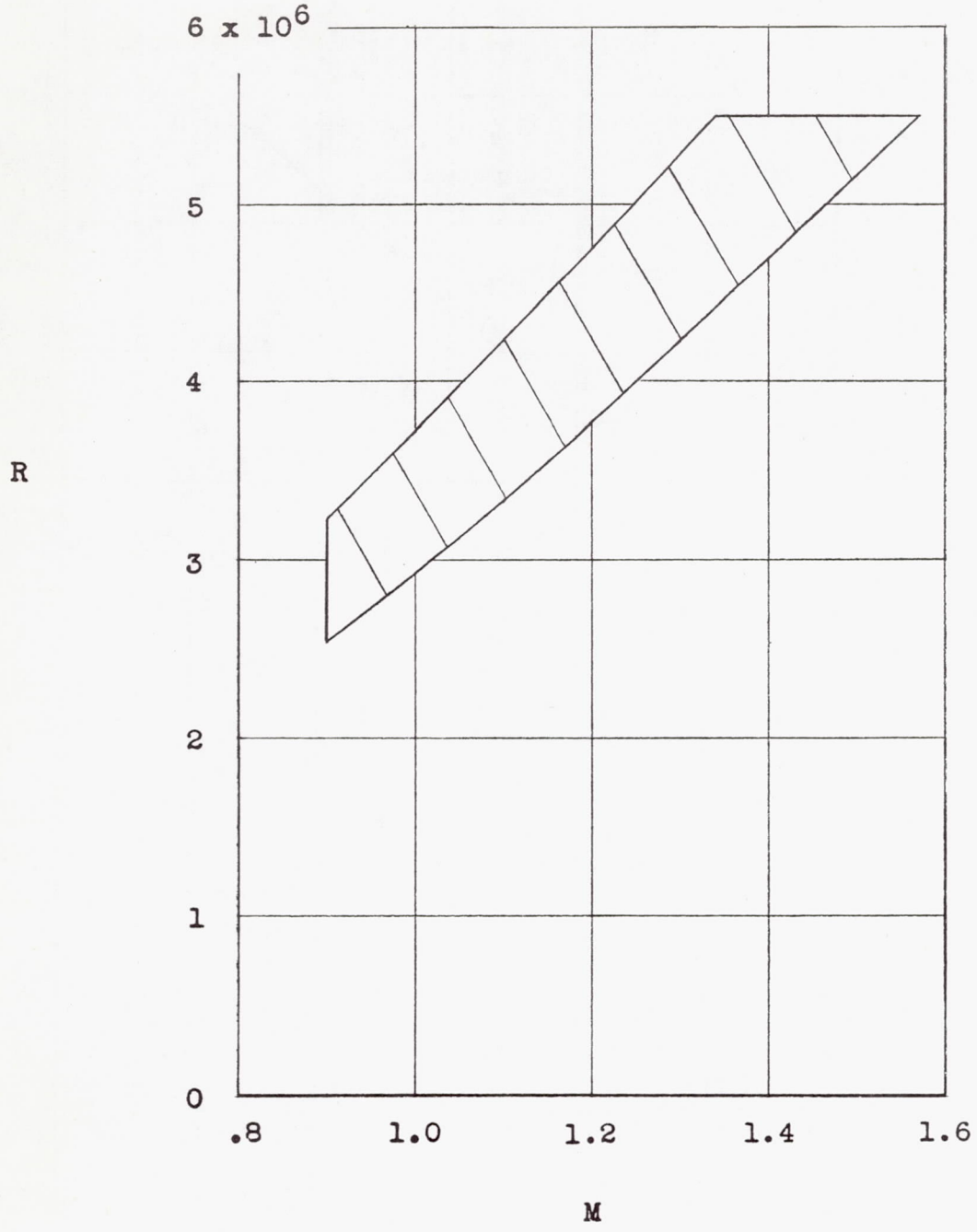

Figure 6.- Range of variation of Reynolds number, based on body maximum diameter, with Mach number for models tested.

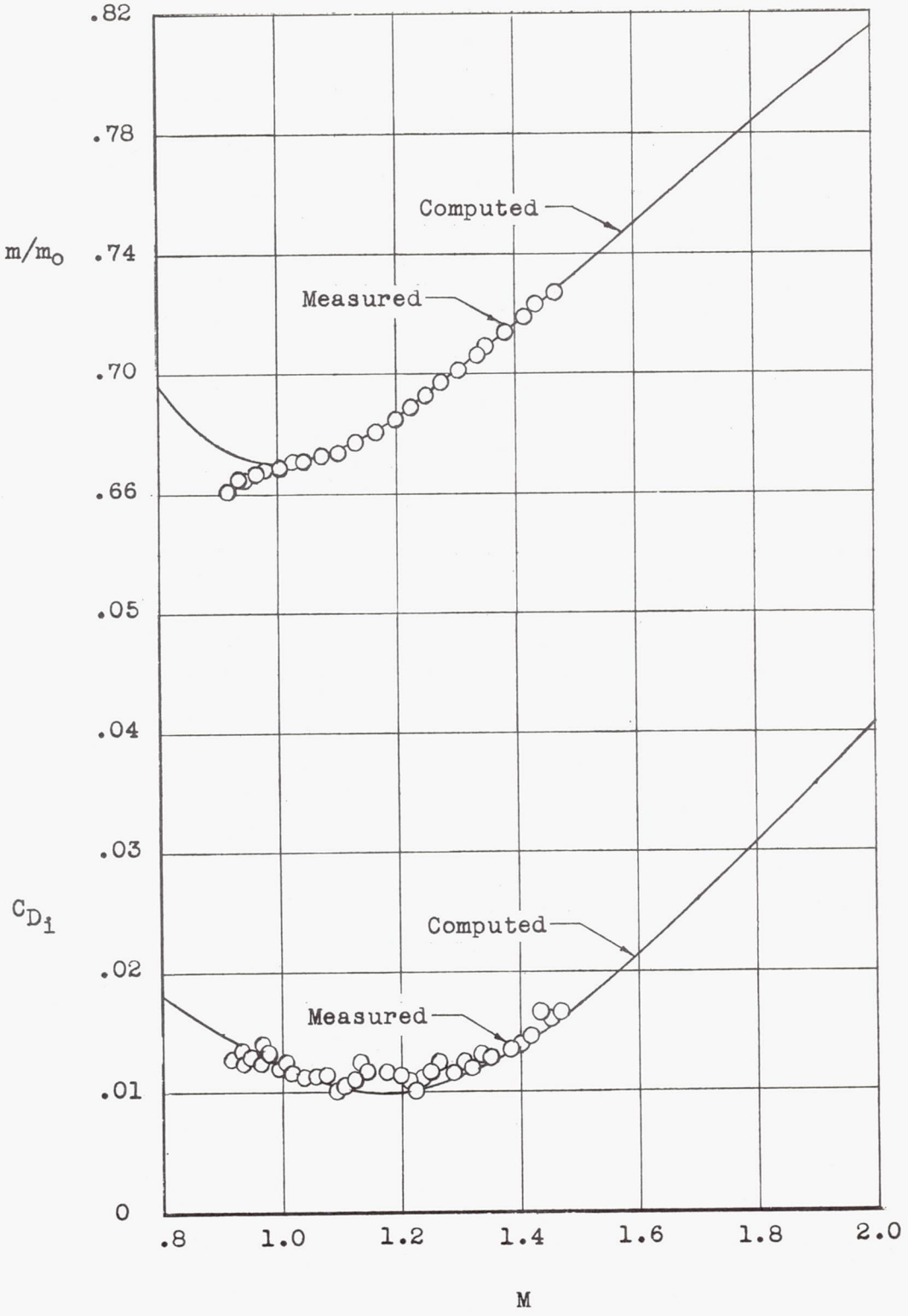

Figure 7.- Variation of internal drag coefficient and mass-flow ratio with Mach number for models with telemeter.

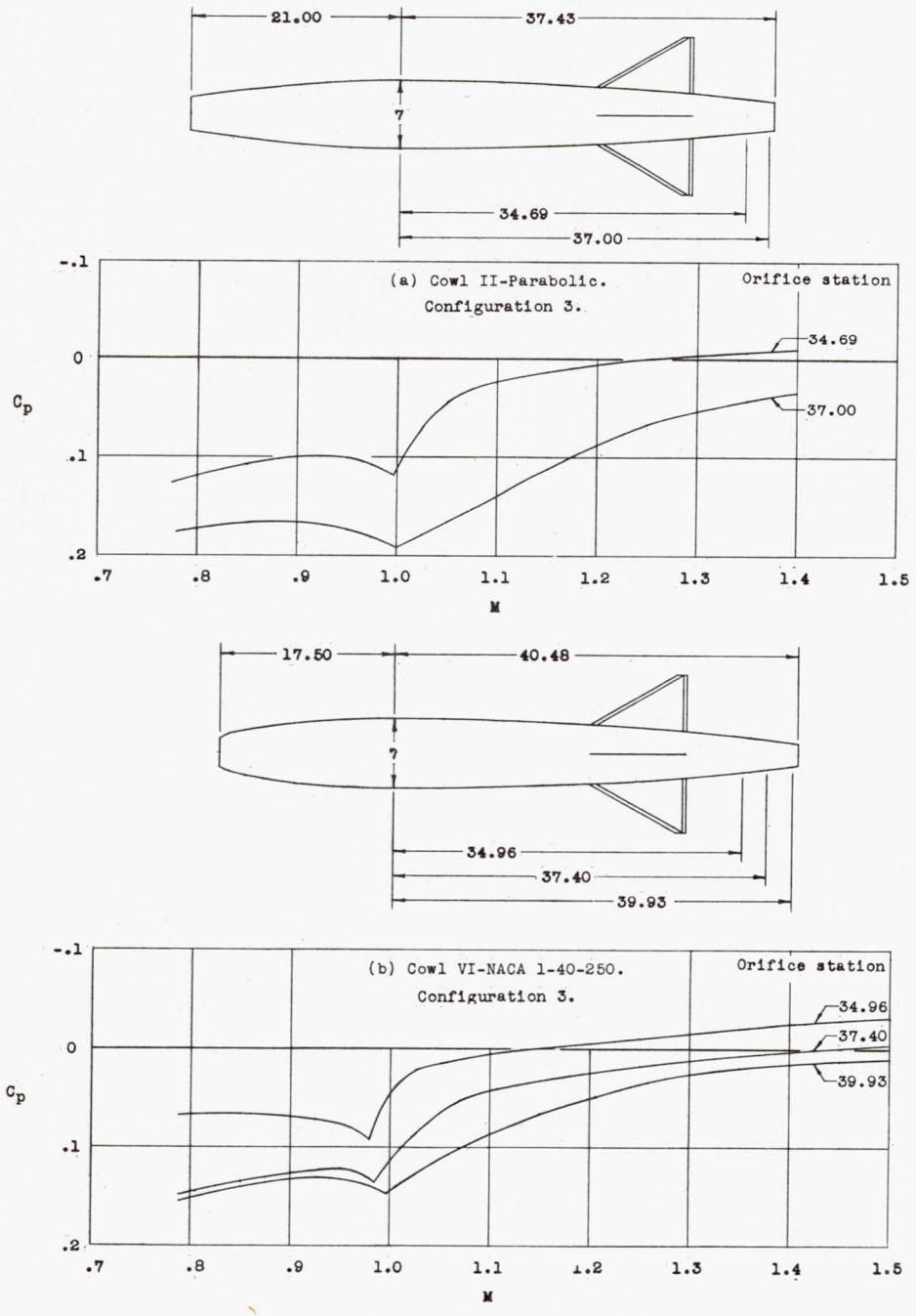

Figure 8.- Variation of pressure coefficient with Mach number at several afterbody stations for two ducted models. All dimensions are in inches.

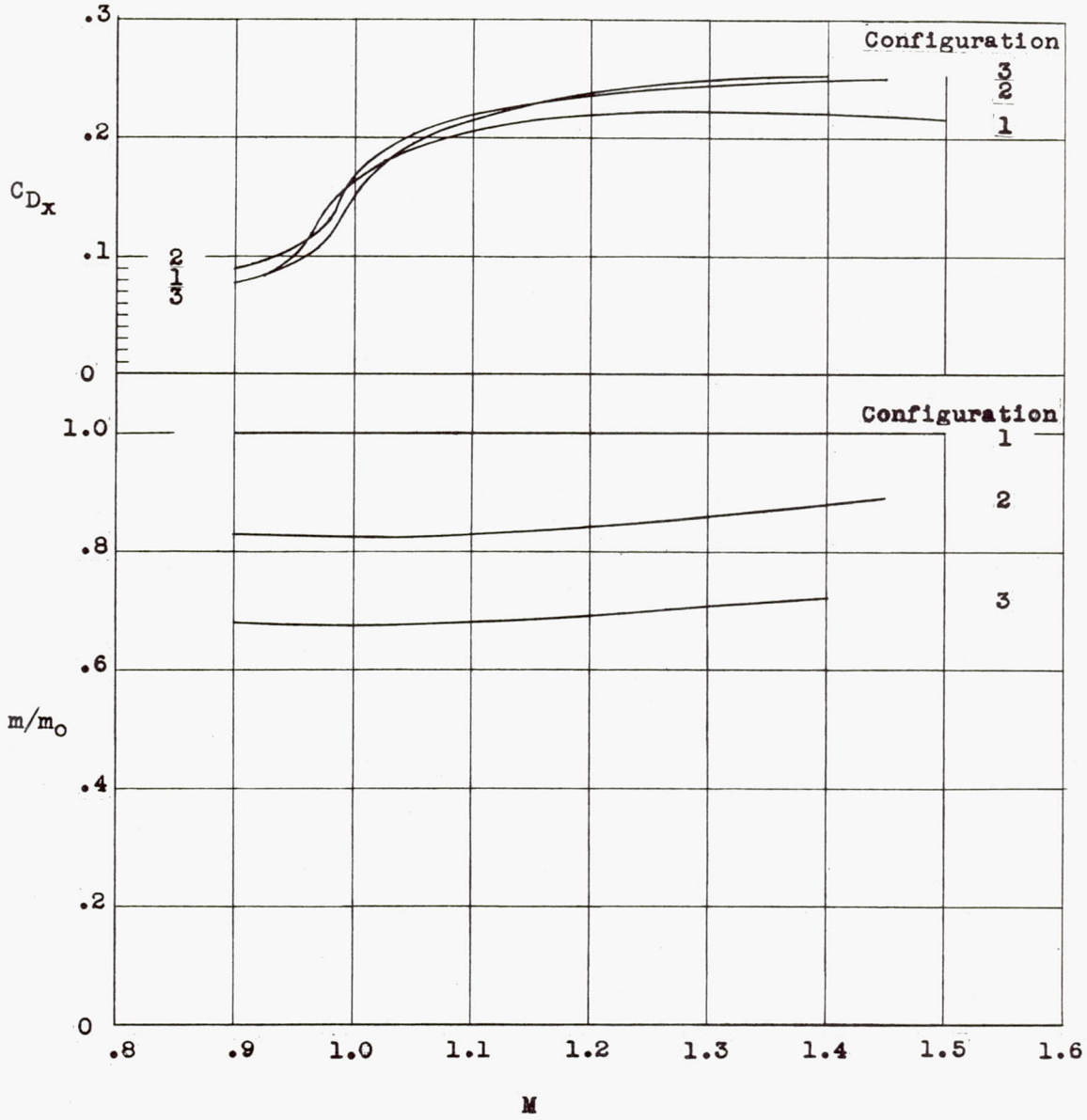

(a) Cowl I; NACA 1-49-300.

Figure 9.- Variation of external drag coefficient and mass-flow ratio with Mach number for the models with various cowl shapes.

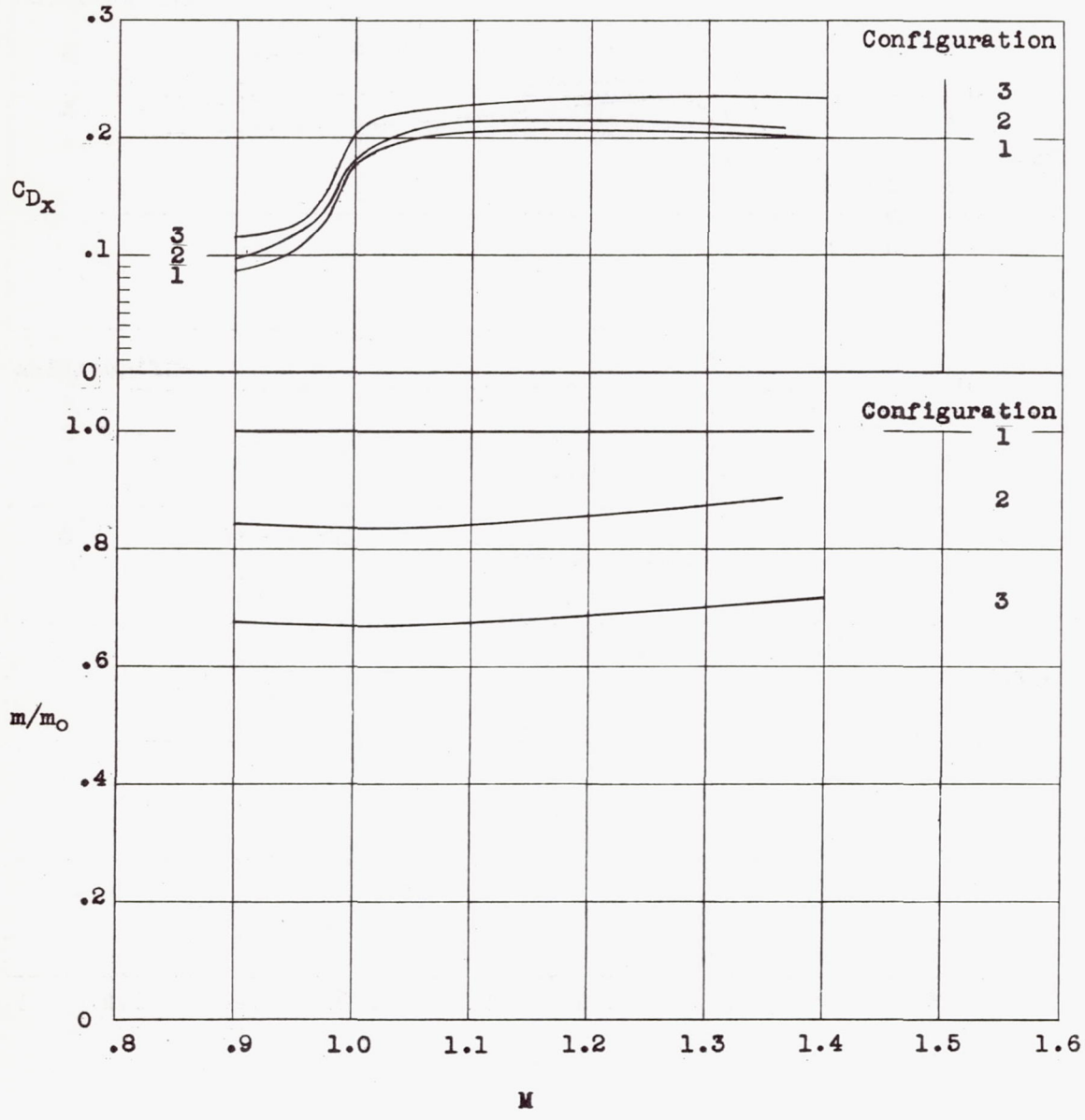

(b) Cowl II; parabolic.

Figure 9.- Continued.

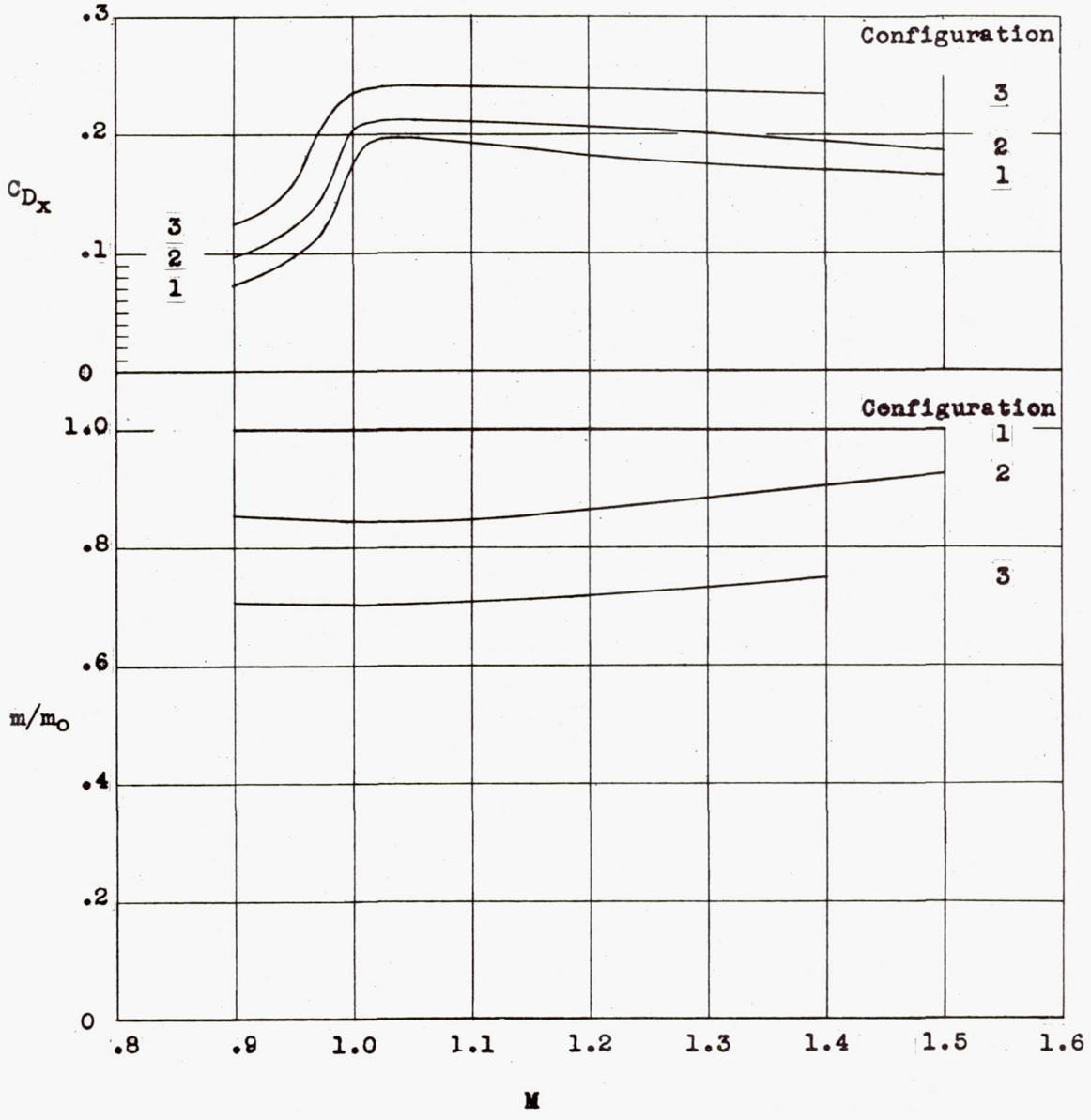

(c) Cowl III; conic, sharp lip.

Figure 9.- Continued.

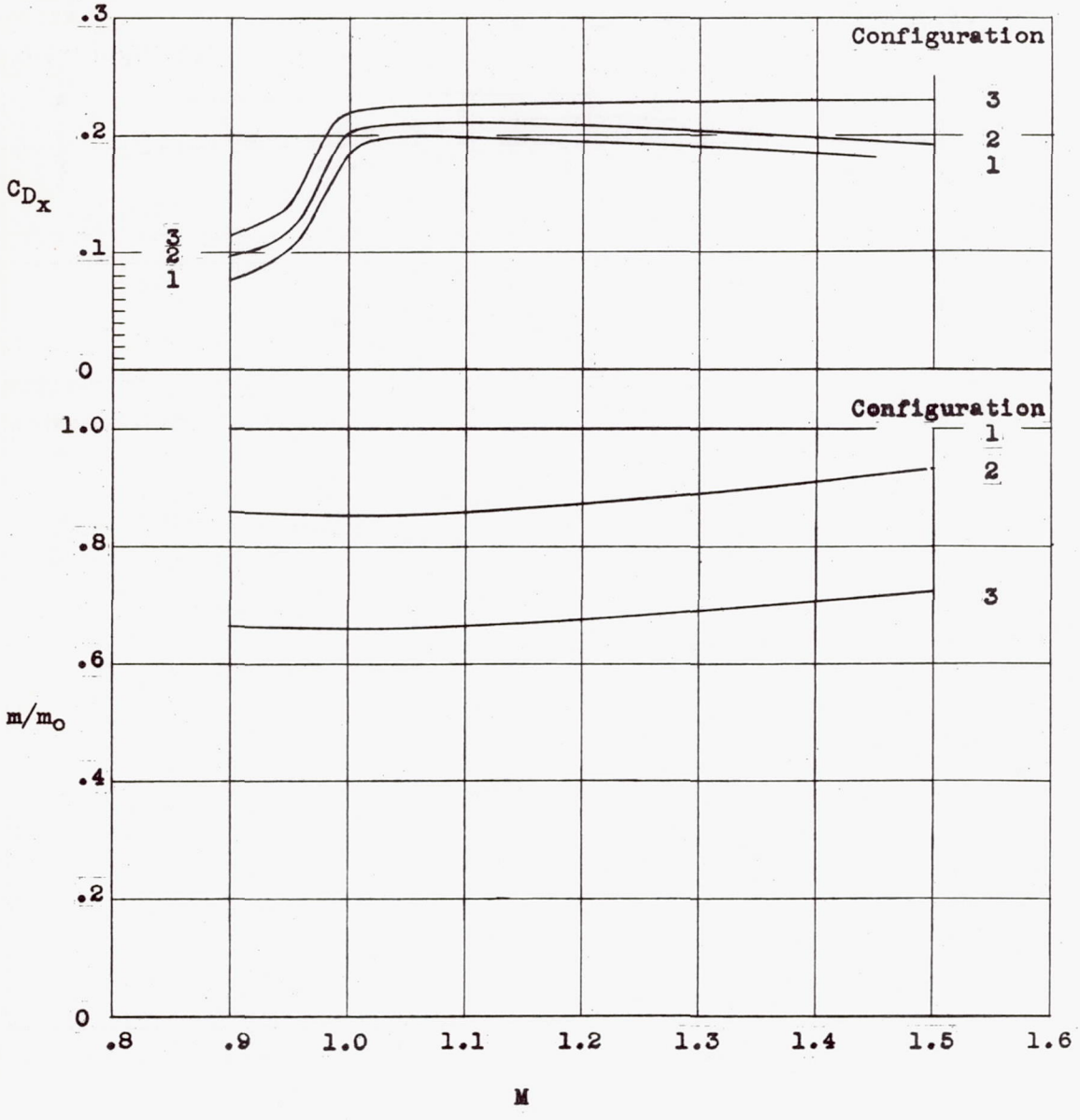

(d) Cowl IV; conic, beveled lip.

Figure 9.- Continued.

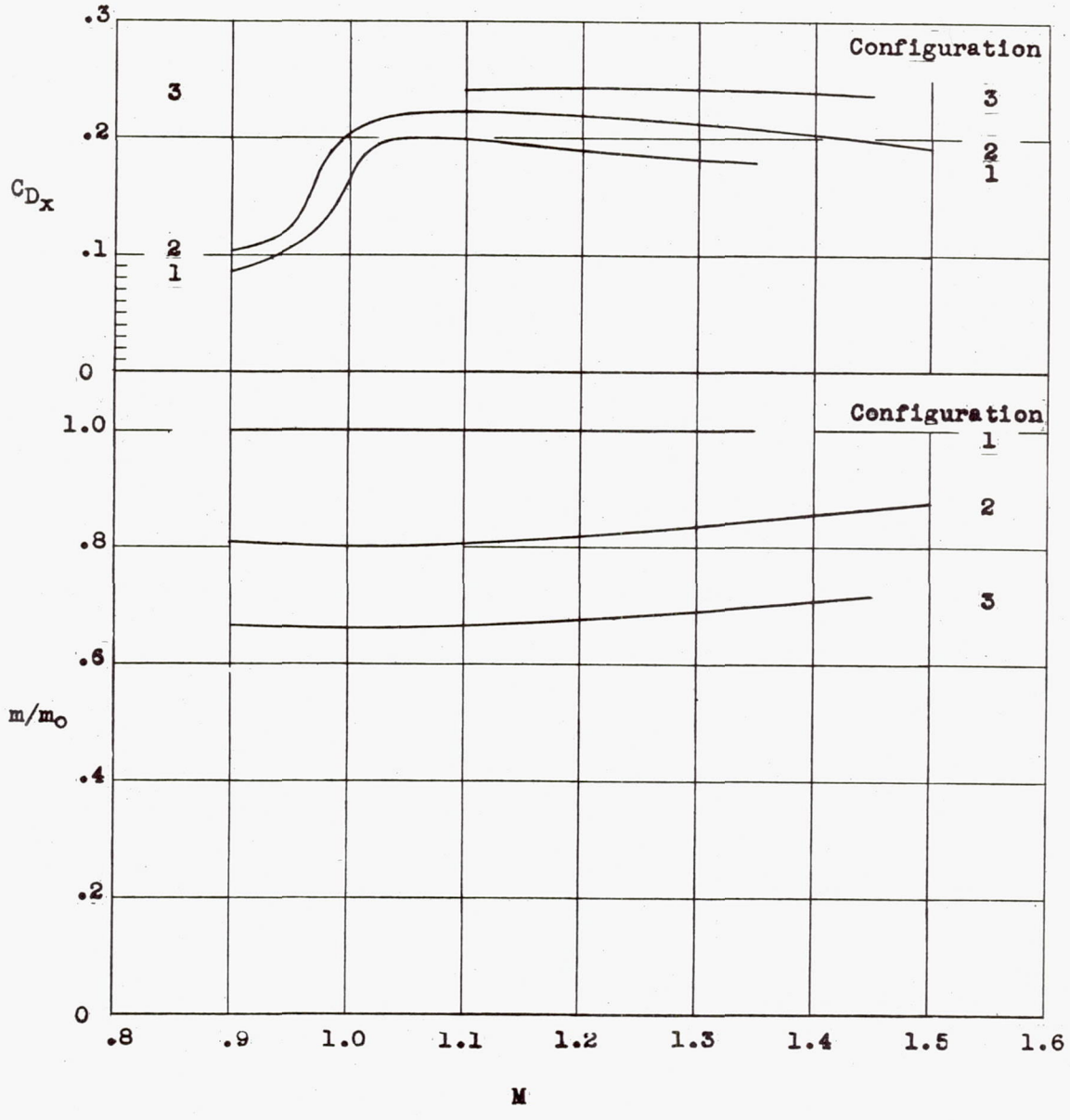

(e) Cowl V; conic, blunt lip.

Figure 9.- Continued.

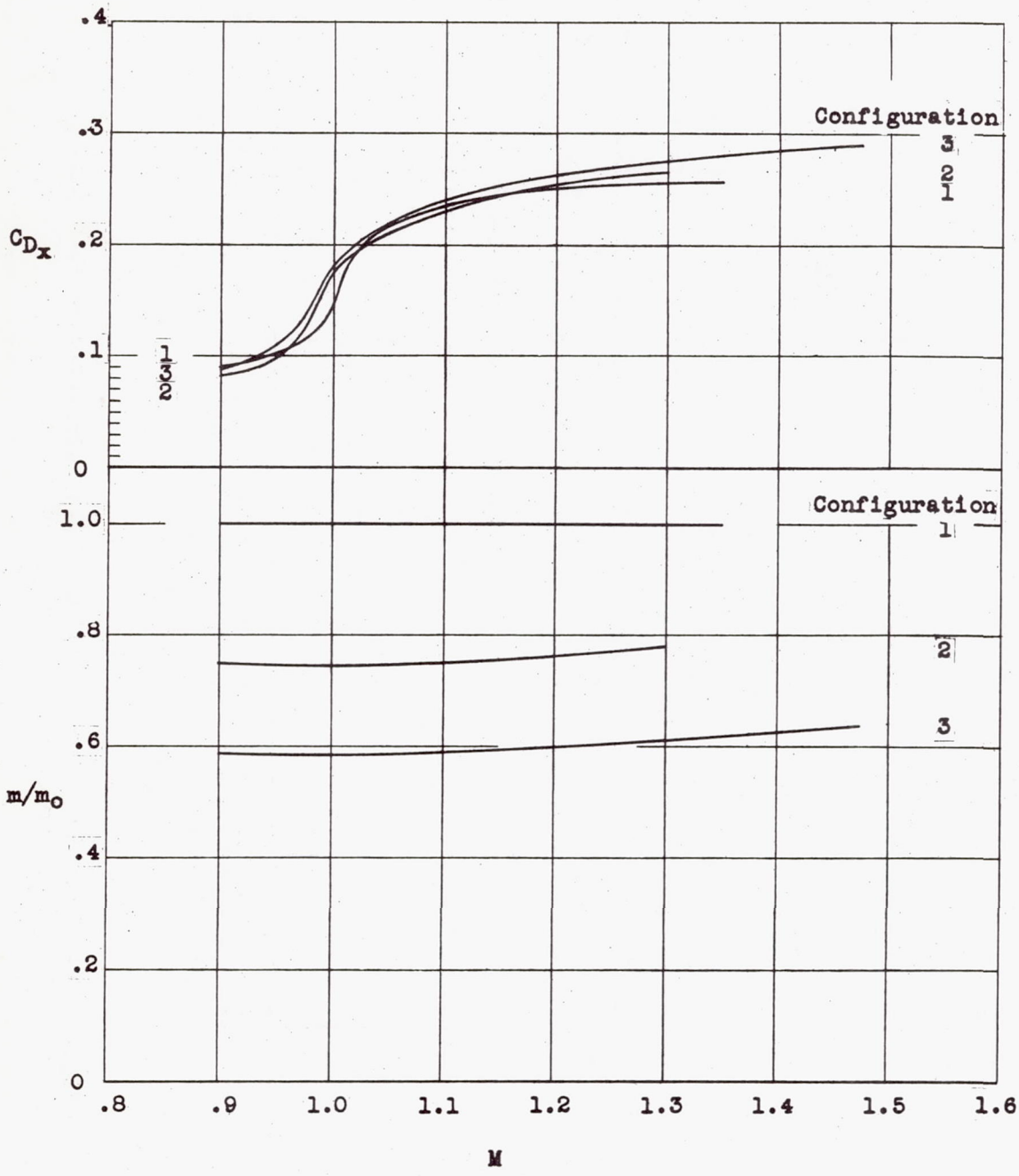

(f) Cowl VI; NACA 1-40-250.

Figure 9.- Concluded.

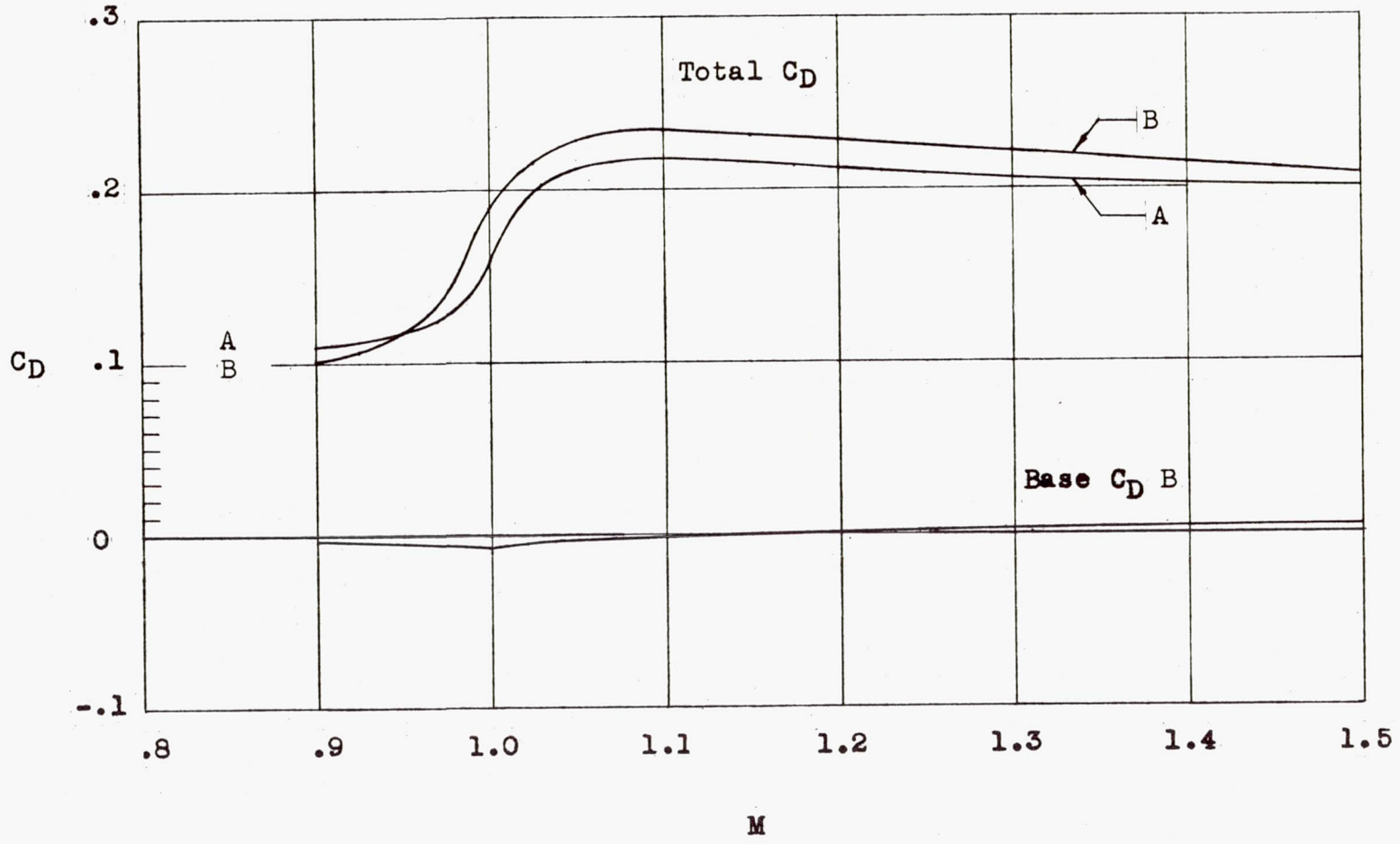

Figure 10.- Variation of total and base drag coefficients with Mach number for the nonducted models.

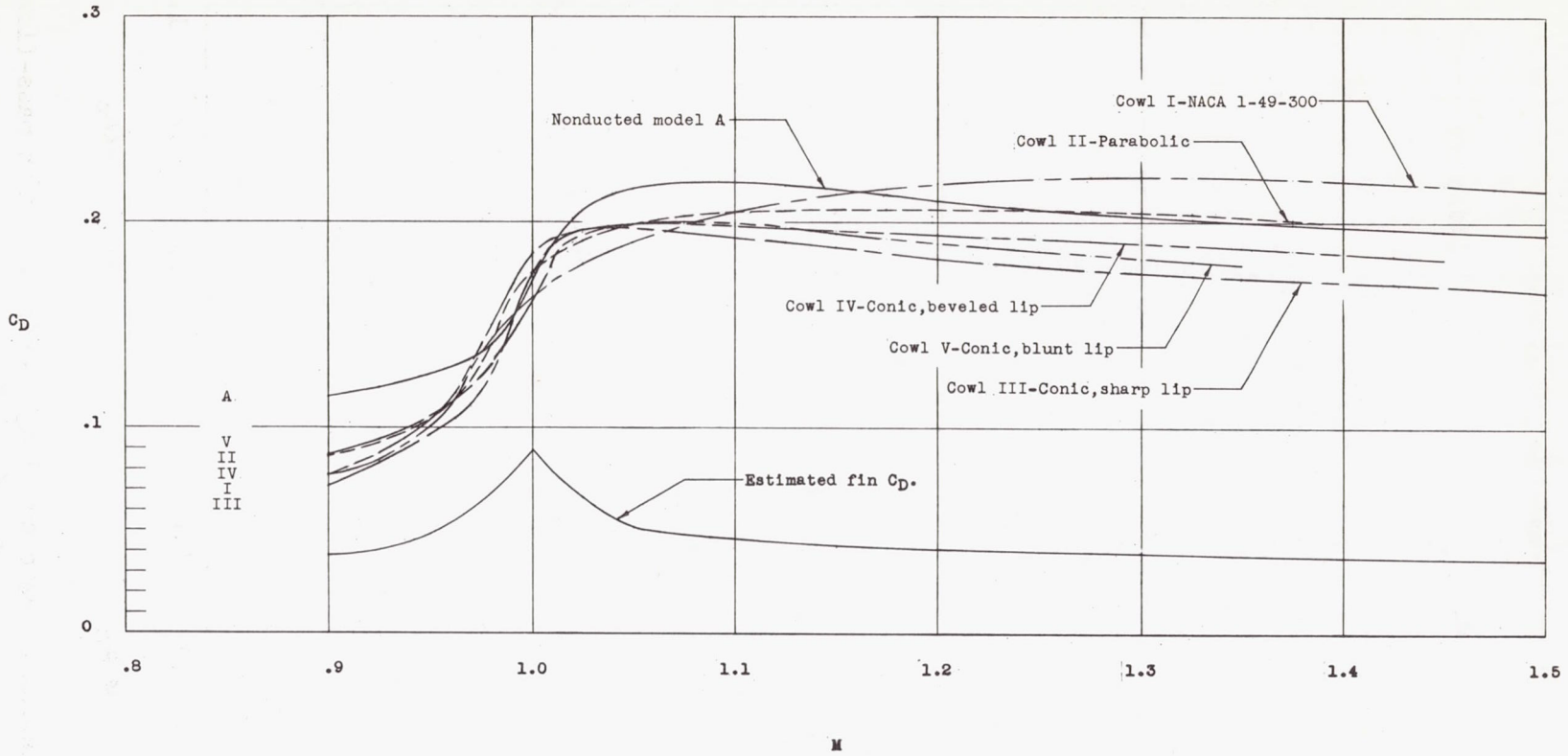

Figure 11.- Variation with Mach number of external drag coefficient for ducted models with various cowls of fineness ratio 3 and total-minus-base drag coefficient for nonducted model A. $\frac{m}{m_o} = 1.0$.

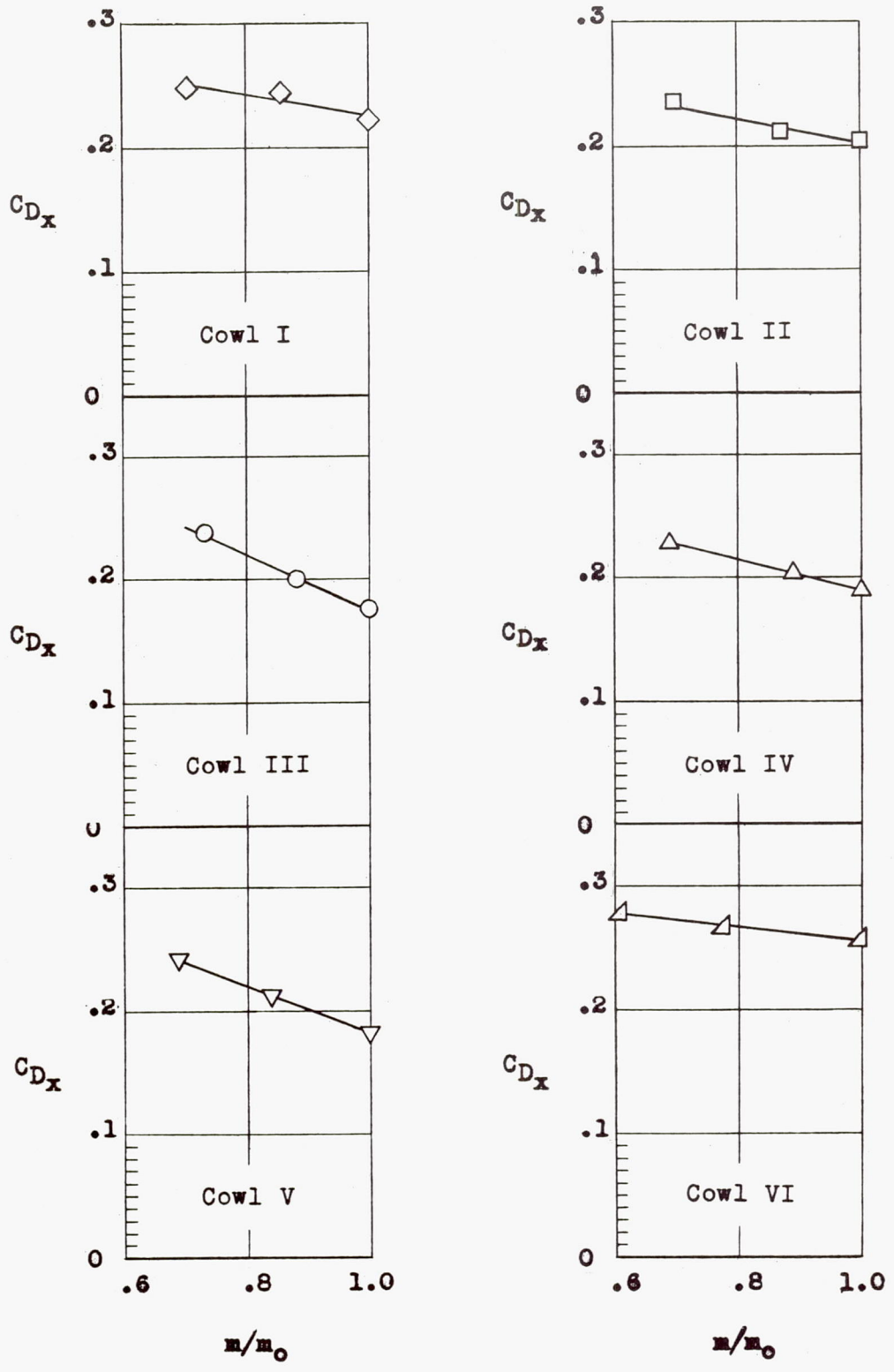

Figure 12.- Variation of external drag coefficient with mass-flow ratio at M = 1.3.

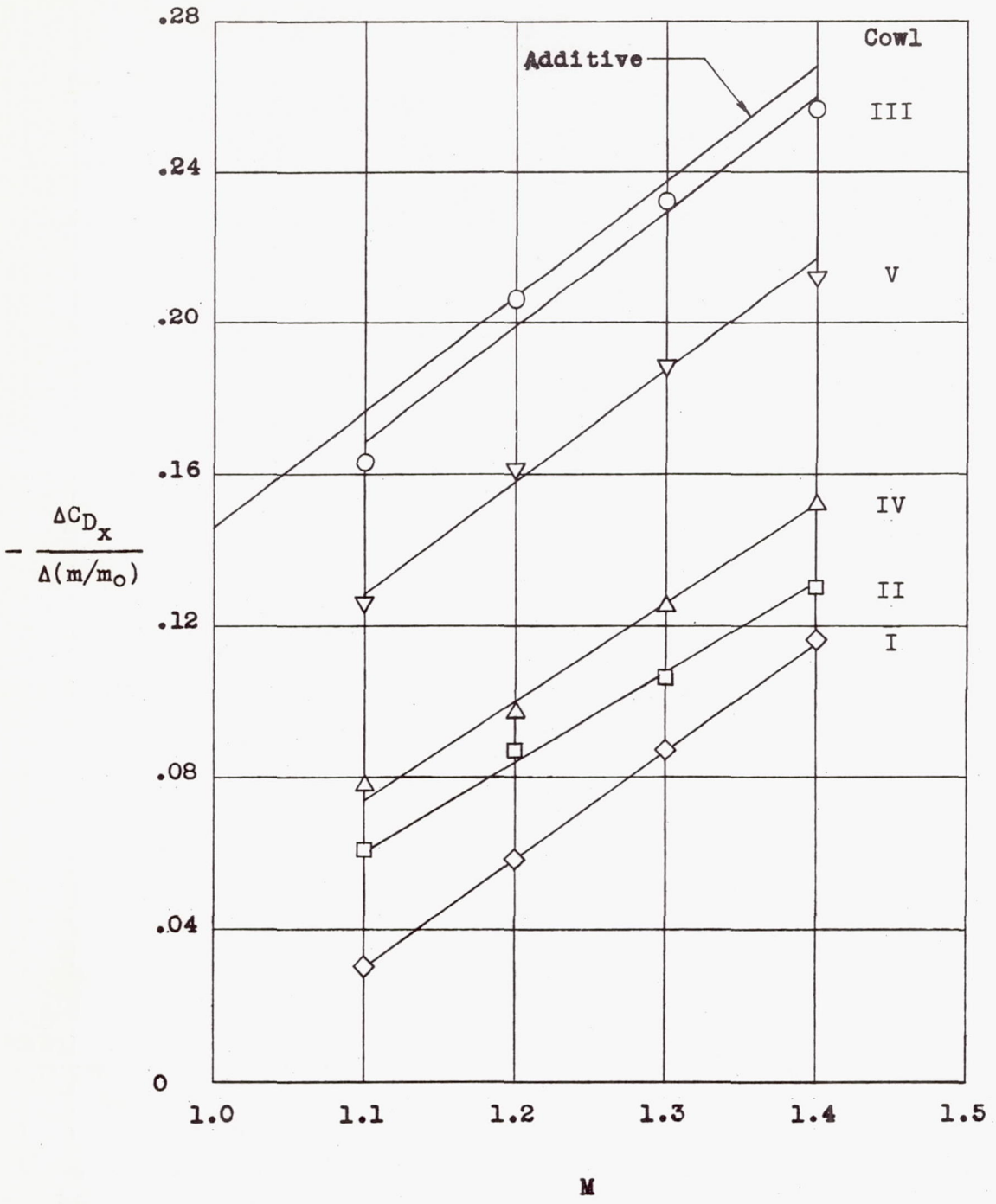

Figure 13.- Variation with Mach number of the change in external drag coefficient with change in mass-flow ratio for models with various cowls of fineness ratio 3.

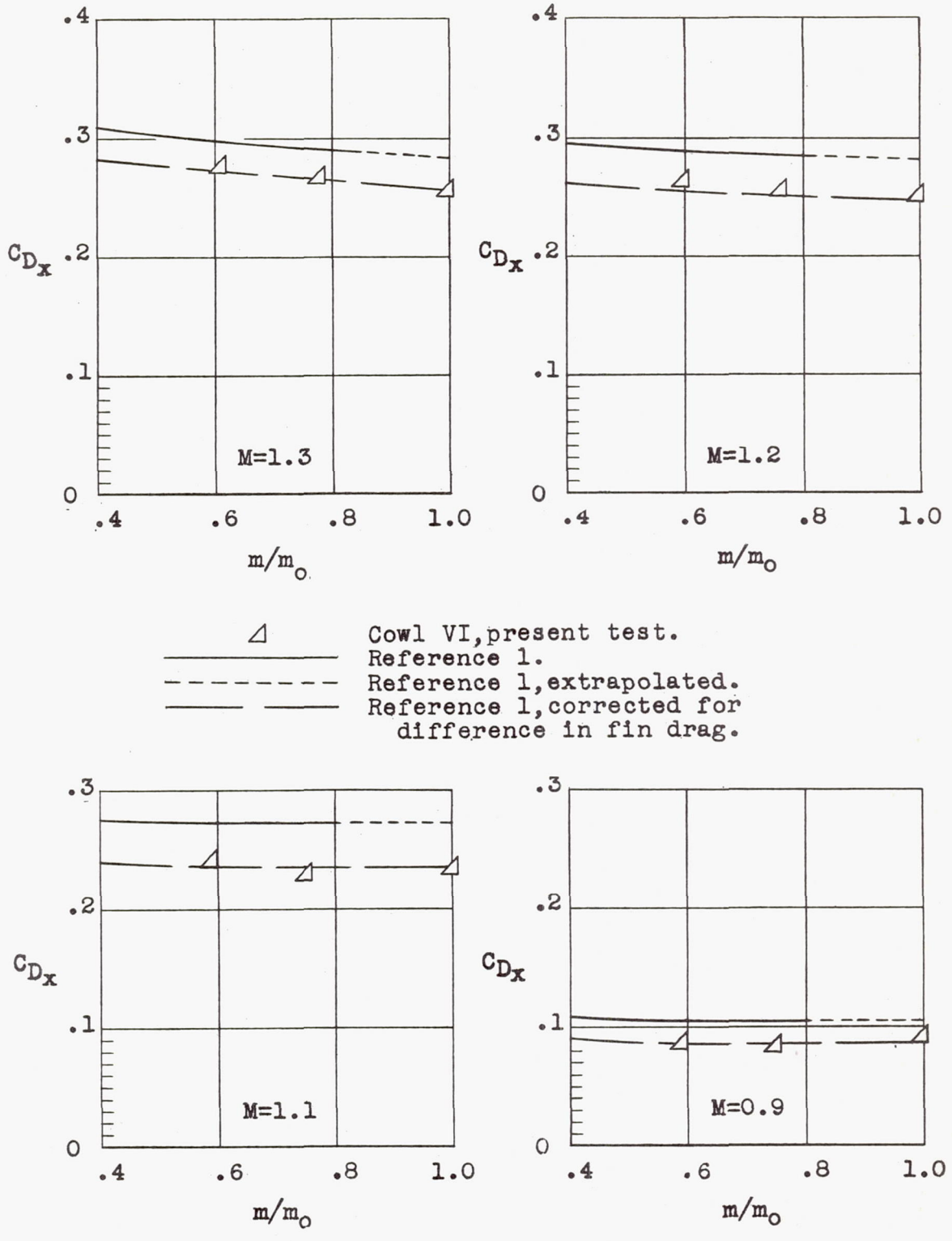

Figure 14.- Comparison of the external drag coefficient of Cowl VI, NACA 1-40-250, with reference 1 at various Mach numbers.

NACA-Langley - 10-22-53 - 325